MSOT/CT/MR imaging Guided and hypoxia Maneuvered Oxygen self-sufficiency radiotherapy based on One-pot MnO_2-$mSiO_2$ @ Au nanoparticle

Supporting Information

Siyu Wang[1], Qing You[1], Jinping Wang[1], Yilin Song[1], Yu Cheng[1], Yidan Wang[1], Shan Yang[1], Lifang Yang[1], Peishan Li[1], Qianglan Lu[1], Meng Yu**[2], Nan Li*[1]

(1 Tianjin Key Laboratory of Drug Delivery ＆ High-Efficiency, School of Pharmaceutical Science and Technology, Tianjin University, 300072, Tianjin, PR China.)

(2 Guangdong Provincial Key Laboratory of new Drug Screening, School of Pharmaceutical Science, Southern Medical University, 510515, Guangzhou, PR China.)

*(Li N.) Corresponding author at: School of Pharmaceutical Science and Technology, Tianjin University, 300072, Tianjin, PR China.

E-mail address: linan19850115@163.com

*(Yu M.) Corresponding author at: School of Pharmaceutical Science, Southern Medical University, 510515, Guangzhou, PR China.

E-mail address: meng4716@126.com

Content

Figure S1 Elements analysis and TEM images of MNH_S

Figure S2 Surface area distribution and multi-point BET plot.

Figure S3 Cumulative surface area and cumulative pore volume distribution.

Figure S4. ^{1}H-NMR spectrum of hyaluronic acid, dopamine and HA-DN complex.

Figure S5. Oxygen generation capability.

Figure S6. Photoacoustic imaging for tumor oxygen generation.

Figure S7. CT imaging for formulation distribution in major organs.

Figure S8 Pharmacokinetic profiles and biodistribution.

Figure S9 T_2-weighted MR images of MnO_2-$mSiO_2$@Au-HA

Figure S10 CT phantom images of Iohexol and MAHNPs

Introduction of photothermal conversion calculation

(a)

Element	Wt %	Atom Wt %
O K	54.85	68.23
Si K	44.51	31.54
Mn K	0.64	0.23
Total	100.00	100.00

(b)

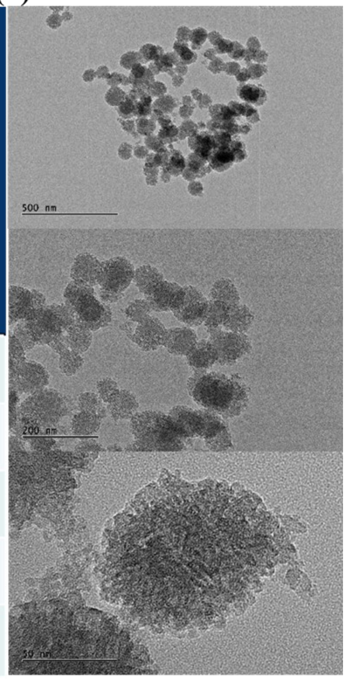

Figure. S1 (a). Elements analysis of $MNH_{S.}$ (b). TEM images of MNH_S scale bar from up to down are 500 nm, 200nm and 20 nm. Table1. The element types O, Si, Mn and the atom weight respectively.

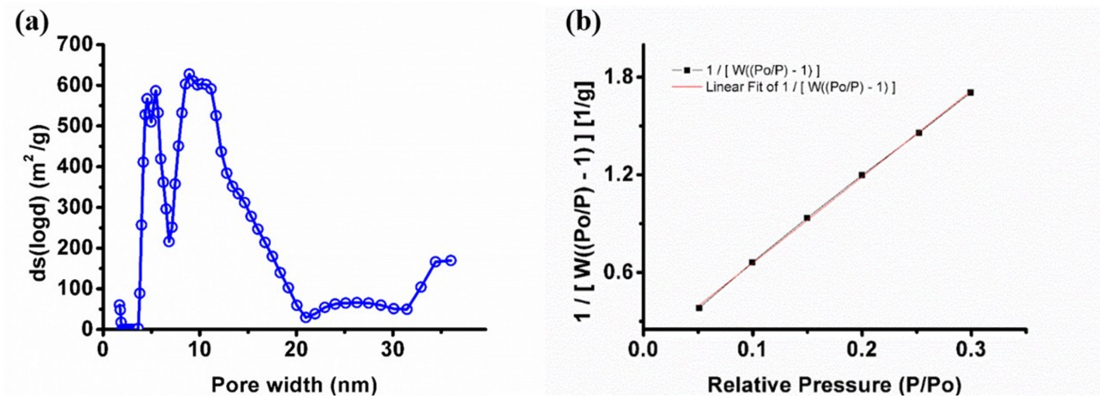

BET Summary	
Slope	5.294 1/g
Intercept	1.289e-01 1/g
Correlation coefficient, R	0.999715
C constant	42.056
Surface Area	642.182 m^2/g

Figure. S2 (a). Surface area distributed by different pore width of MnO_2-$mSiO_2$ nanohybrids. (b). Multi-point BET plot of MnO_2-$mSiO_2$ nanohybrids. Table.2. BET data summary.

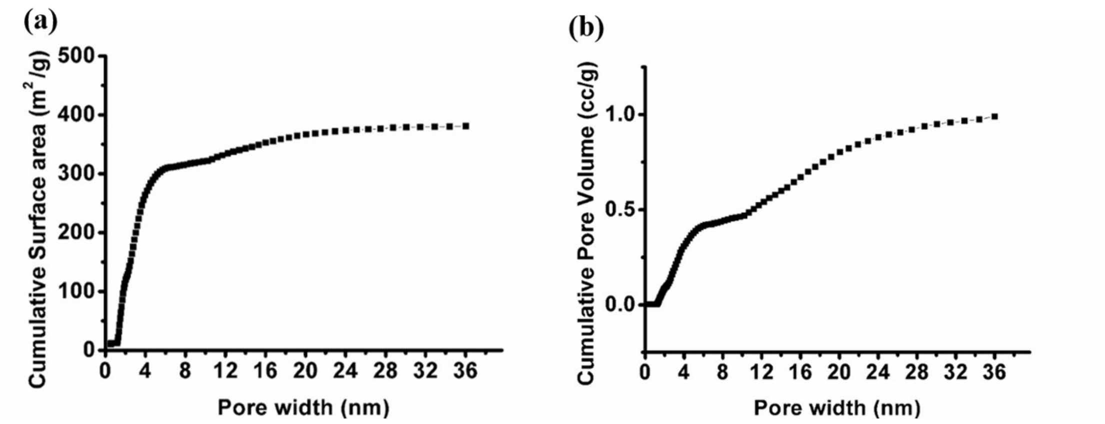

DFT method Summary	
Pore volume	0.989 cc/g
Surface area	381.083 m^2/g
Lower confidence limit	0.524 nm
Pore width (Mode(dLog))	16.015 nm

Figure. S3 (a). Cumulative surface area of MnO_2-SiO_2 nanohydrids. (b) Cumulative pore volume distributed by different pore width of MnO_2-SiO_2 nanohybrids. Table3. DFT method Summary.

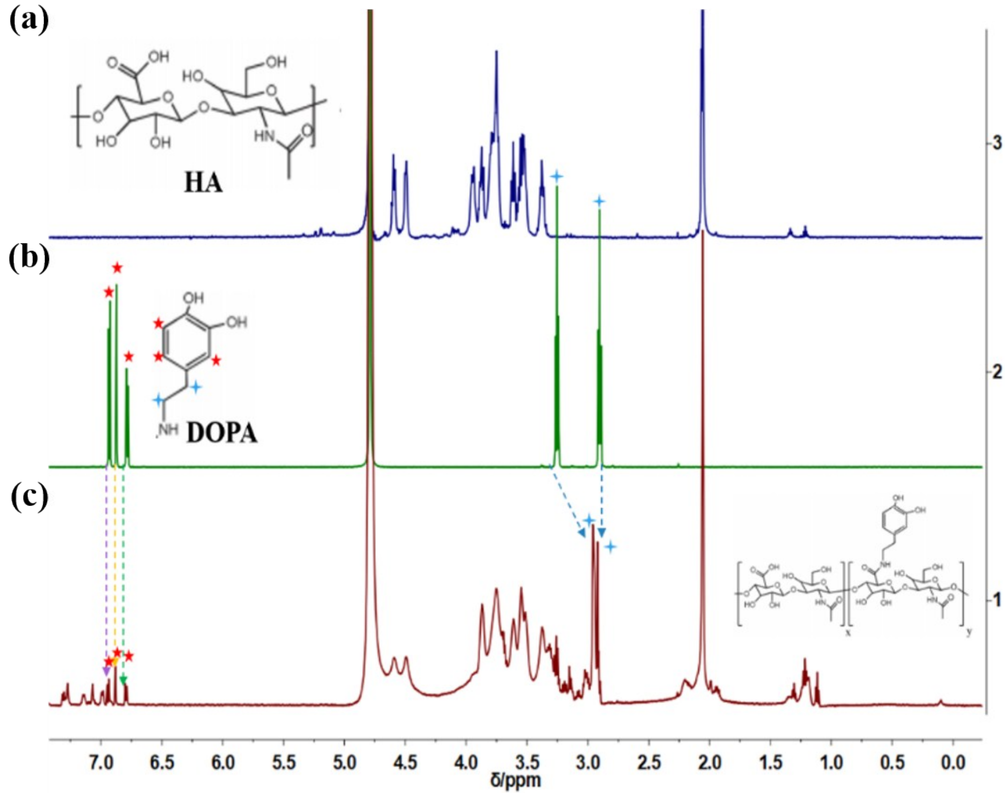

Figure. S4 (a). ^{1}H-NMR spectrum of the unmodified hyaluronic acid (b) ^{1}H-NMR spectrum of dopamine (c). ^{1}H-NMR spectrum of HA-DN complex.

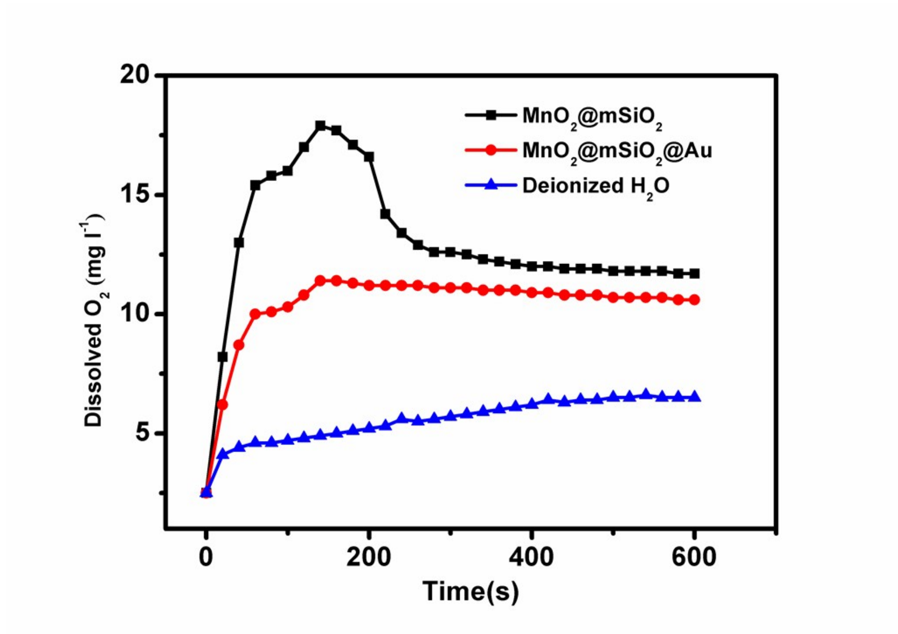

Figure. S5 Oxygen generation capability of different formulations.

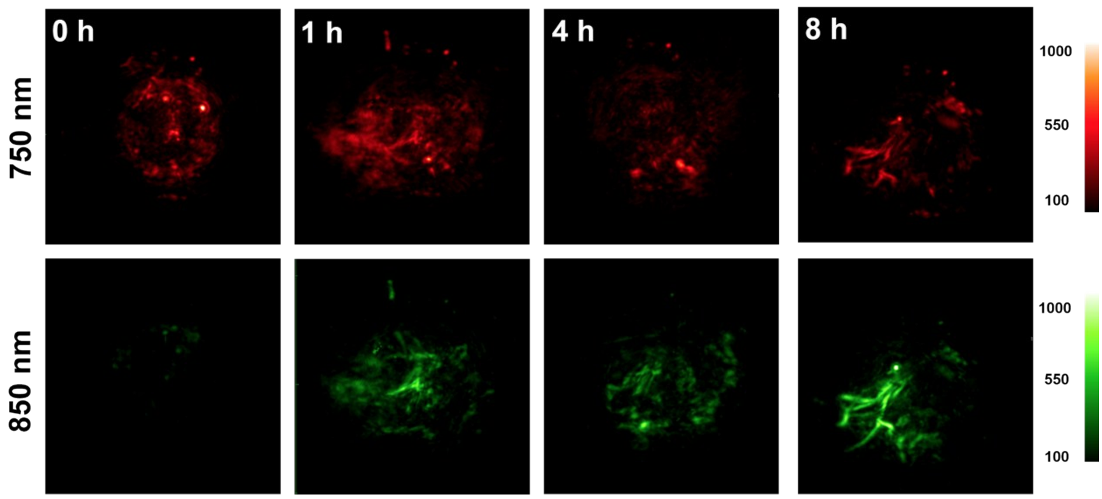

Figure. S6 Photoacoustic imaging for tumor oxygen generation

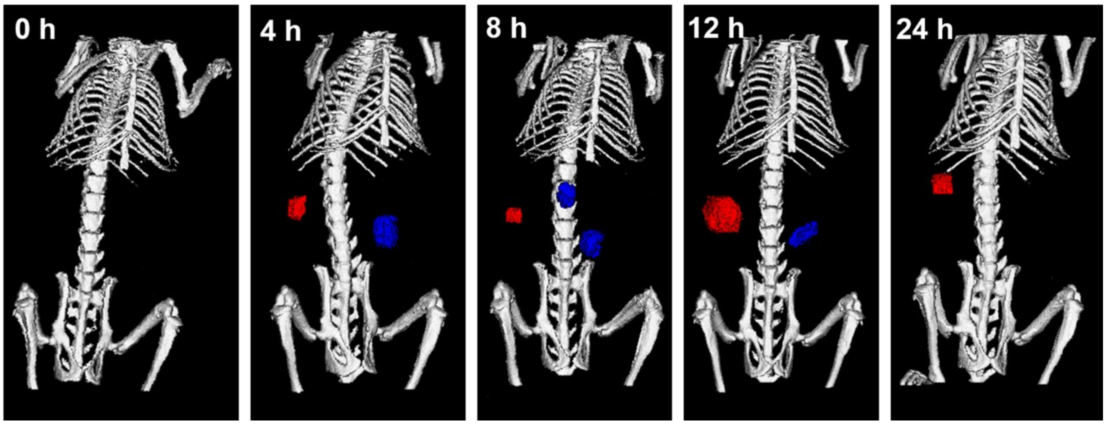

Figure. S7. CT imaging for formulation distribution in major organs after 24 h injection. The circled sections represent the tumor sites.

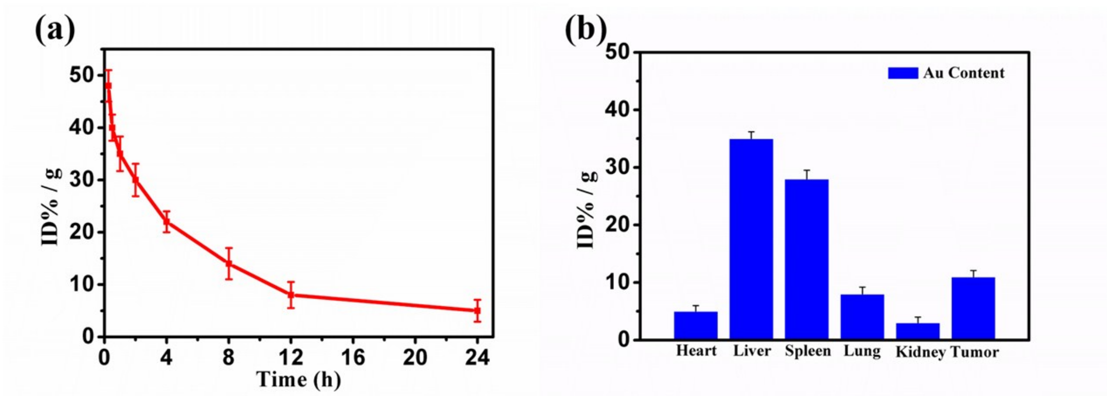

Figure. S8 (a). Pharmacokinetic profiles of MnO_2-mSiO_2@Au-HA nanoparticles following intravenous administration by measureing Au concentrations. (b). Biodistribution in major organs after intravenously injection of MnO_2-mSiO_2@Au-HA nanoparticles.

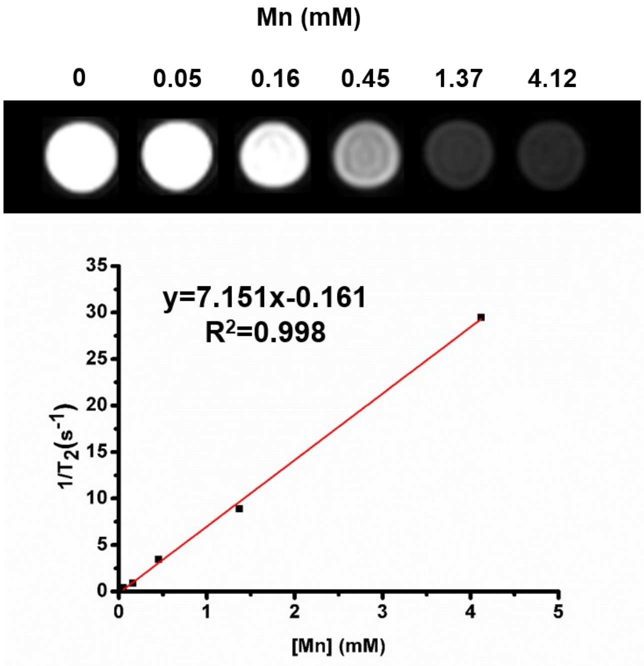

Figure S9. T_2-weighted MR images of MnO_2-$mSiO_2$@Au-HA at varying Mn^{2+}concentrations. Lower is the linear relationship between the T_2 relaxation rate ($1/T_2$) and Mn^{2+} concentrations in MnO_2-$mSiO_2$@Au-HA aqueous solutions.

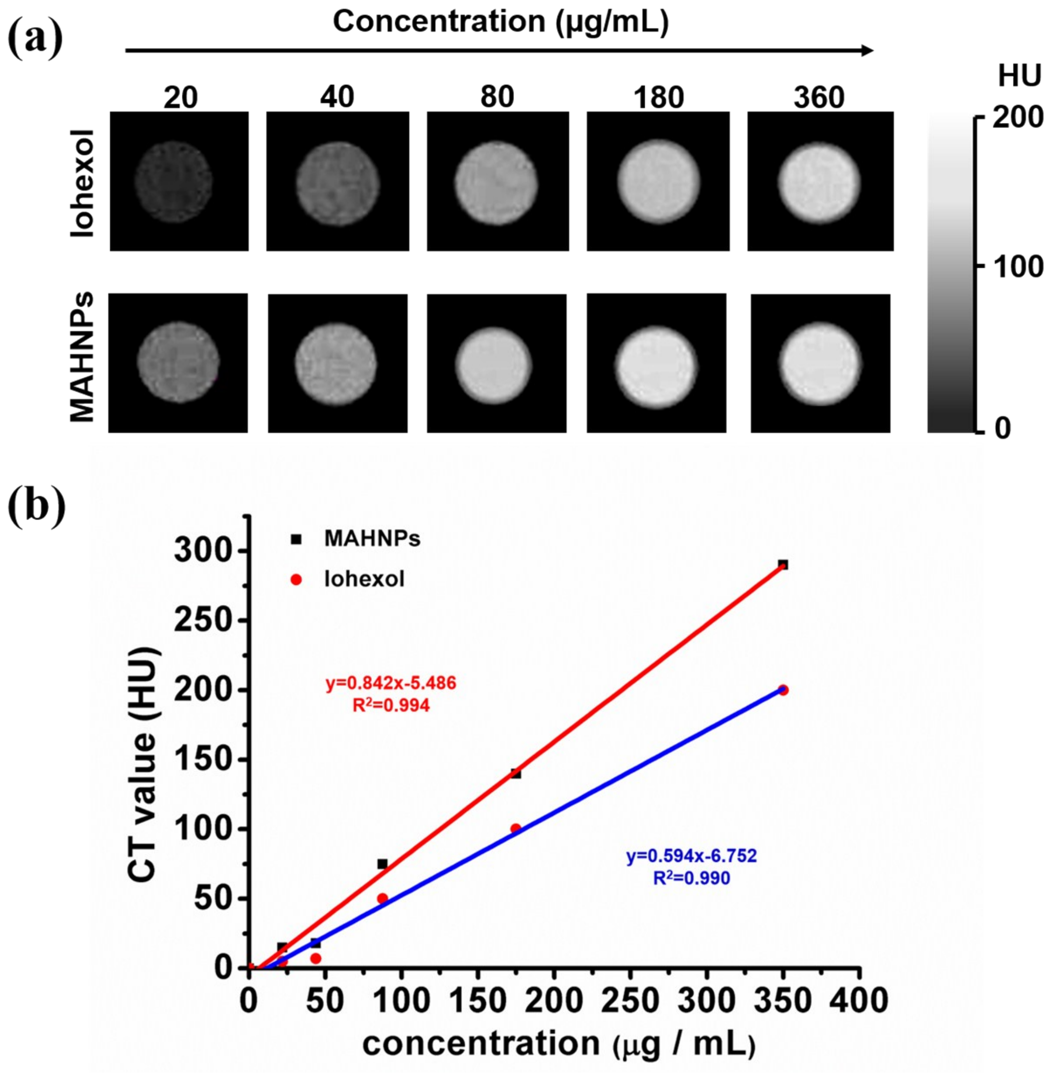

Figure. S10 (a). CT phantom images of Iohexol (upper panel) and MAHNPs (lower panel) at different I or Au concentrations. (b). CT values of MAHNPs and Iohexol with different Au or I concentrations.

The Calculation of the photothermal conversion efficiency was determined by the following steps according to the references[1-3].

Firstly, the aqueous solution of the MnO_2-$mSiO_2$@Au-HA nanoparticles (100 ppm) underwent continuous irradiation of 808 nm laser (1.5 W/cm^2) until steady state temperature was reached. Then the laser was shut off, and the aqueous solution was naturally cooled to environment temperature. The temperature change of the aqueous solution was recorded (Figure. 2g). The η value was calculated as follows:

$$\eta = \frac{hs(T_{Max} - T_{Surr}) - Q_S}{I(1 - 10^{-A808})} \qquad (1)$$

Where h is the heat transfer coefficient, S is the surface area of the container, and the value of hs is obtained from the Eq. (4) and Figure 2h. The maximum steady temperature (T_{max}) was 63.1 °C and environmental temperature (T_{Surr}) was 25.9 °C. The laser power I used in irradiation was 1.5 W/cm^2. The absorbance of the MnO_2-$mSiO_2$@Au-HA nanoparticles at 808 nm was 0.534. Q_{Dis} is heat dissipated from the light absorbed by the solvent and container. A dimensionless parameter θ is calculated as followed:

$$\theta = \frac{T - T_{\mathrm{Surr}}}{T_{Max} - T_{Surr}} \qquad (2)$$

A sample system time constant τ_s can be calculated as Eq. (3)

$$t = -\tau_s \ln(\theta) \qquad (3)$$

According to figure 2g, τ_s was obtained to be 166.97 s.

$$hs = \frac{m_D C_D}{\tau_s} \qquad (4)$$

In addition, m_D is 0.5 g and C_D is 4.2 J/g·°C in the experiment.

Q_S is heat dissipated from the light absorbed by the container itself, and it was determined independently to be 3.5 mW using a container containing pure water. Thus, substituting according values of each parameters to Eq. 1, the 808 nm laser photothermal conversion efficiency (η) of the MnO_2-$mSiO_2$@Au-HA nanoparticles can be calculated to be 25.38%.

[1] J. Xiao, S. Fan, F. Wang, L. Sun, X. Zheng, C. Yan, *Nanoscale* 2014, **6**, 4345-4351.

[2] X. Liu, B. Li, F. Fu, K. Xu, R. Zou, Q. Wang, B. Zhang, Z. Chen, J. Hu, *Dalton Trans.*, 2014, **43**, 11709-11715.

[3] B. Li, Q. Wang, R. Zou, X. Liu, K. Xu, W. Li, J. Hu, *Nanoscale,* 2014, **6**, 3274-3282.